



Comparison of transcriptomic profiles between HFPO-DA and prototypical PPAR α , PPAR γ , and cytotoxic agents in wild-type and PPAR α knockout mouse hepatocytes

Melissa M. Heintz ^{1,*} William D. Klaren ¹ Alexander W. East,¹ Laurie C. Haws,² Steven R. McGreal,³ Rebecca R. Campbell,³ Chad M. Thompson⁴

¹ToxStrategies LLC, Asheville, North Carolina 28801, USA

²ToxStrategies LLC, Austin, Texas 78731, USA

³BioIVT LLC, Kansas City, Kansas 66103, USA

⁴ToxStrategies LLC, Katy, Texas 77494, USA

*To whom correspondence should be addressed at ToxStrategies, LLC, 31 College Place, Suite B118, Asheville, NC 28801. E-mail: mheintz@toxstrategies.com.

Abstract

Recent *in vitro* transcriptomic analyses for the short-chain polyfluoroalkyl substance, HFPO-DA (ammonium, 2,3,3,3-tetrafluoro-2-(heptafluoropropoxy)-propanoate), support conclusions from *in vivo* data that HFPO-DA-mediated liver effects in mice are part of the early key events of the peroxisome proliferator-activated receptor alpha (PPAR α) activator-induced rodent hepatocarcinogenesis mode of action (MOA). Transcriptomic responses in HFPO-DA-treated rodent hepatocytes have high concordance with those treated with a PPAR α agonist and lack concordance with those treated with PPAR γ agonists or cytotoxic agents. To elucidate whether HFPO-DA-mediated transcriptomic responses in mouse liver are PPAR α -dependent, additional transcriptomic analyses were conducted on samples from primary PPAR α knockout (KO) and wild-type (WT) mouse hepatocytes exposed for 12, 24, or 72 h with various concentrations of HFPO-DA, or well-established agonists of PPAR α (GW7647) and PPAR γ (rosiglitazone), or cytotoxic agents (acetaminophen or d-galactosamine). Pathway and predicted upstream regulator-level responses were highly concordant between HFPO-DA and GW7647 in WT hepatocytes. A similar pattern was observed in PPAR α KO hepatocytes, albeit with a distinct temporal and concentration-dependent delay potentially mediated by compensatory responses. This delay was not observed in PPAR α KO hepatocytes exposed to rosiglitazone, acetaminophen, d-galactosamine. The similarity in transcriptomic signaling between HFPO-DA and GW7647 in both the presence and absence of PPAR α *in vitro* indicates these compounds share a common MOA.

Keywords: HFPO-DA (GenX); PFAS; peroxisome proliferator-activated receptor α (PPAR α); mode of action (MOA); hepatocytes; transcriptomics.

The liver is a common target of toxicity in rodent studies following oral exposure to per- and polyfluoroalkyl substances (PFAS) (Costello *et al.*, 2022). However, different modes of action (MOAs) have been hypothesized for PFAS-mediated liver effects in rodents, likely due to the diversity in chemical structures across PFAS (eg, interchain linkages, carbon chain length). For example, the MOA for liver lesions in mice exposed to the short-chain PFAS, HFPO-DA (ammonium, 2,3,3,3-tetrafluoro-2-(heptafluoropropoxy)-propanoate; CASRN 62037-80-3), has been evaluated in detail using mechanistic and phenotypic data from *in vivo* rodent studies. The current weight of evidence supports that HFPO-DA-mediated liver effects in mice are part of the early key events of the peroxisome proliferator-activated receptor alpha (PPAR α) activator-induced rodent hepatocarcinogenesis MOA (Heintz *et al.*, 2023). In our companion article (Heintz *et al.*, 2024), *in vitro* transcriptomic analyses for HFPO-DA support the MOA conclusions from *in vivo* data by demonstrating that transcriptomic responses in HFPO-DA-treated mouse and rat hepatocytes have high concordance with responses in rodent hepatocytes treated with the prototypical PPAR α agonist, GW7647. Moreover, there is

a lack of concordance of responses in rodent hepatocytes treated with the PPAR γ agonist, rosiglitazone, and cytotoxic agents, acetaminophen and d-galactosamine (Heintz *et al.*, 2024). Just as GW7647 served as a positive control for PPAR α activation, these latter agents served as positive controls for comparing transcriptomic responses/signatures to assess alternate MOAs involving PPAR γ or cytotoxicity that have been hypothesized for HFPO-DA-mediated liver effects in mice (USEPA, 2021).

The established PPAR α MOA (currently under development as an adverse outcome pathway) for rodent liver tumors consists of 4 key events: (1) PPAR α activation, (2) alteration in cell growth pathways, (3) perturbation of cell growth and survival, and (4) selective clonal expansion of preneoplastic foci cells (Corton *et al.*, 2014, 2018). To further investigate the role of Key Event 1 (PPAR α activation) in the MOA for HFPO-DA in mouse liver and elucidate whether HFPO-DA-mediated transcriptomic responses in mouse liver are PPAR α -dependent, an additional *in vitro* transcriptomic study was conducted using a similar experimental design as described previously (see companion publication) but with primary PPAR α knockout (KO) and wild-type (WT) B6129SF2/

J mouse hepatocytes. The PPAR α KO mouse is a well-characterized model used to investigate the role of PPAR α and molecular mechanisms of putative PPAR α activators (Attema et al., 2022; Foreman et al., 2009; Nakagawa et al., 2012; Rosen et al., 2008; Wolf et al., 2008); however, few studies have been conducted in PPAR α KO hepatocytes. Upon treatment with known PPAR α agonists, PPAR α KO mice lack induction of β -oxidation enzyme gene expression, peroxisome proliferation, and hepatomegaly, but increase hepatic lipid accumulation (Lee et al., 1995). Herein, transcriptomic responses in WT and PPAR α KO mouse hepatocytes were compared across treatments with HFPO-DA, GW7647, rosiglitazone, acetaminophen, or d-galactosamine following exposure from 12 to 72 h (Figure 1). Results from this study provide novel insight into the mechanisms of PPAR activators and may explain, in part, why some findings in PPAR α KO mouse hepatocytes share some similarity to WT counterparts.

Materials and methods

Chemicals

Ammonium perfluoro(2-methyl-3-oxahexanoate) (HFPO-DA; CASRN 62037-80-3; 95% purity) was purchased from Manchester Organics Ltd (Runcorn, Cheshire, United Kingdom). GW7647 (CASRN 265129-71-3; \geq 98% purity) was purchased from Cayman Chemical Company (Ann Arbor, Michigan). Rosiglitazone (CASRN 122320-73-4; 98.9% purity), acetaminophen (CASRN 103-90-2; \geq 99% purity), and d-galactosamine (CASRN 1772-03-8; \geq 99% purity) were purchased from Sigma Aldrich (St Louis, Missouri).

Primary hepatocyte isolation and culture

Mouse hepatocytes were isolated from the livers of 11-week-old male B6129SF2/J mice (stock no. 101045) and 11-week-old male PPAR α -null mice (B6; 129S4-Ppara^{tm1Gonz}/J, stock no. 008154) purchased from The Jackson Laboratory (Bar Harbor, Maine). Primary hepatocytes from male mice were used for the *in vitro* assay herein based on findings from previous toxicity studies in rodents demonstrating greater sensitivity to HFPO-DA-mediated liver effects in males (Chappell et al., 2020; Heintz et al., 2022; Thompson et al., 2019). As described in Lee et al. (1995), PPAR α -null mice were generated by a targeted disruption of the ligand-binding domain (ie, deletion of 83 base pairs in exon 8; see Lee et al., 1995 for details) of the mouse PPAR α (mPPAR α) gene, rendering the mPPAR α gene nonfunctional. Although nonfunctional, mPPAR α RNA was detected by Lee et al. (1995) in these mice at very low expression levels. However, Lee et al. (1995) used Western blotting to confirm the lack of mPPAR α protein expression, and lack functional protein activity was demonstrated by the inability to activate downstream PPAR α target genes (Lee et al., 1995). PPAR α -null mice are considered constitutive KO mice (ie, PPAR α is nonfunctional in the entire animal), thus primary hepatocytes from PPAR α -null mice will be referred to as PPAR α KO hepatocytes. B6129SF2/J mice were used as the genetic background strain for PPAR α KO mice¹ and are referred to as WT hepatocytes.

¹ Note: A single specific genetic background strain for B6;129S4-Ppara^{tm1Gonz}/J does not exist, however, either B6129SF2/J or C57BL/6J strains have been determined to be appropriate background strains based on what is known regarding the B6;129S4-Ppara^{tm1Gonz}/J genome. In the companion publication, transcriptomic responses for each chemical investigated were consistent (especially for PPAR α activators, HFPO-DA and GW7647) across hepatocytes from different mouse strains (CD-1 and B6129SF2/J) and rodent species (ie, rats), indicating that the genetic differences between rodent strains/species did not impact the overall transcriptomic response/MOA for the chemicals investigated.

Hepatocytes from both mouse genotypes were isolated using a 2-step enzymatic digestion of liver tissue as described in Mudra and Parkinson (2001). Hepatocyte viability was determined by trypan blue (0.04%; Millipore Sigma, St Louis, Missouri) exclusion and was \geq 79%. Primary hepatocytes were plated in a collagen-sandwich configuration on 48-well plates and maintained according to the methods described in the companion publication.

Hepatocyte treatments

Using 48-well plates, WT and PPAR α KO mouse hepatocytes were seeded at densities of 0.6×10^6 cells/ml and 0.5×10^6 cells/ml, respectively. After a 24-h acclimatization period, hepatocytes from each genotype were treated for 12, 24, or 72 h with supplemented modified Eagle's medium containing solvent control in the presence or absence of HFPO-DA (0.1, 5, 50, or 500 μ M) or one of the following positive controls: GW7647 (0.01, 0.1, 1, or 10 μ M), rosiglitazone (0.01, 0.1, 1, or 10 μ M), acetaminophen (0.3, 1, 3, or 10 mM), or d-galactosamine (0.3, 1, 3, or 10 mM). Deionized water (1%) served as the solvent control for HFPO-DA and dimethylsulfoxide (0.1%; cell culture grade; Sigma Aldrich) served as the solvent control for the remaining test chemicals. Treatment solutions were replaced every 24 h. For each genotype, treatment groups were performed in triplicate wells for 12 and 72 h treatment durations, and quadruplicate wells for the 24-h treatment duration.

Hepatocyte cultures were visualized and photographed at 24, 48, and 72 h following treatment to document morphological integrity according to the methods described in the companion publication.

Cytotoxicity assay

The release of lactate dehydrogenase (LDH) into culture medium indicates loss of cell membrane integrity and was used to estimate cytotoxicity. LDH release was measured using a commercial kit (Roche Diagnostics GmbH, Mannheim, Germany) according to the manufacturer's directions. Additional details regarding LDH assay methodology are provided in the companion publication. Cytotoxicity in a treatment group was determined based on measurements of percent LDH release \geq 25% in combination with changes in hepatocyte morphology indicative of cytotoxicity. A preliminary cytotoxicity assay was performed to select treatment concentrations used in the present study (data not shown).

RNA preparation and sequencing

Following treatment with HFPO-DA or positive controls (ie, GW7647, rosiglitazone, acetaminophen, or d-galactosamine) for 12, 24, or 72 h, hepatocytes were lysed using TempO-Seq Enhanced Lysis Buffer and processed according to the TempO-Seq protocol by BioSynder Technologies (Carlsbad, California), as previously described (Yeakley et al., 2017). Resultant DNA libraries were sequenced using a HiSeq 2500 Ultra-High-Throughput Sequencing System (Illumina, San Diego, California).

Sequencing data processing and assessment of quality

Raw sequencing data (ie, FASTQ files) were analyzed according to the TempO-Seq data analysis pipeline described in Yeakley et al. (2017). For each mouse genotype, the output from the TempO-Seq pipeline was a table containing the number of sequenced reads per TempO-Seq probe per sample, with each probe representing a gene-specific sequence. Samples were excluded from the downstream analyses if either or both of the following

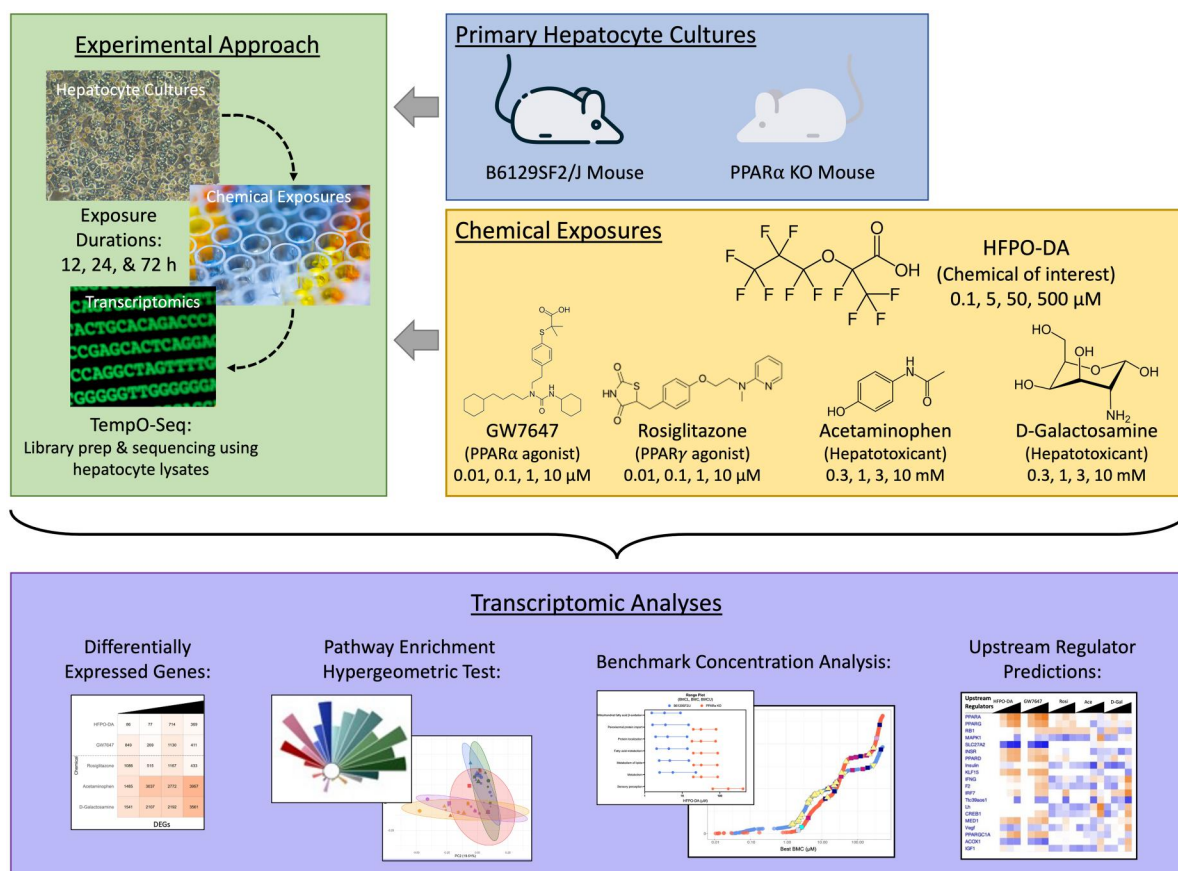


Figure 1. Experimental study design.

exclusion criteria were met: (1) overall sequencing depth (total number of reads across all probes) lower than 2 SDs below the mean sequencing depth across all samples from the same genotype; (2) total number of sequenced probes lower than 2 SDs below the mean number of probes sequenced per sample from the same genotype. Count data from all samples that were not excluded were used for further comparative analyses.

Differential gene expression analyses

Sequencing data were analyzed using packages (described here and in subsequent sections) in the R software environment, version 4.3.1 (cran.r-project.org/). The DESeq2 R package (v1.40.2) (Love et al., 2014) was used to normalize data and account for sample-to-sample variation in sequencing depth within each mouse genotype. Fold-change and differentially expressed probes (DEPs) associated with chemical treatment were determined within DESeq2 by conducting statistical comparisons between treatment groups and controls from the same mouse genotype and treatment duration. DEPs were defined as those with a false discovery rate (FDR) <10%, based on *p*-values adjusted for multiple testing using the Benjamini and Hochberg (BH) procedure (Love et al., 2014); differentially expressed genes (DEGs) were identified from respective DEPs, as some genes (but not all) are represented by multiple probes in the TempO-Seq assay. The expression levels of 21 398 mouse genes as measured by 30 146 mouse probes were reported from the TempO-Seq assay for each sample.

Identification of pathway-level responses to treatment

Biological pathways associated with transcriptomic responses in mouse hepatocytes following treatment with HFPO-DA or

positive controls were identified by gene set enrichment analysis as described in the companion publication. Enrichment of sets of genes (ie, the constituents of a molecular signaling pathway) was evaluated using the hypergeometric test method for overrepresentation. Significant DEGs (ie, genes with an FDR of <10% as described above) for each treatment group, timepoint, and mouse genotype were tested for overrepresentation among the gene sets in the canonical pathway subcollection using the Fisher combined probability test function within the Platform for Integrative Analysis of Omics data (PIANO) R package (v2.16.0) (Varemo et al., 2013). Gene sets with an FDR <5% were considered significantly enriched.

Gene set aggregation and visualizations

A comparative targeted gene set analysis was conducted according to the methods described in the companion publication (Heintz et al., 2024) to better understand the types of gene sets that were significantly enriched across chemical treatment groups. Briefly, the top 10 chemical-gene interactions from the Comparative Toxicogenomics Database (CTD; <https://ctdbase.org/>; accessed November 2022) for HFPO-DA and each of the positive control chemicals were used to identify and select gene sets that contained one or more of these top interacting genes. From the list of gene sets containing one or more interacting genes, adjusted *p*-values for significantly enriched gene sets (FDR <5%) across all treatment groups were reverse log-scaled, with non-significant pathways set equal to zero, and the gene set with the lowest adjusted *p*-value (ie, most significant) set equal to 1. Within each treatment group, gene sets containing the same interacting gene were aggregated by summing the reverse

log-scaled adjusted *p*-values. Lastly, the summed totals for each interacting gene for each treatment group and timepoint were scaled from 0 to 1 using internal and external scaling methods. Internal scaling was defined as scaling the summed totals for each interacting gene relative to each other within the same treatment group and timepoint. External scaling was defined as scaling the summed totals for the same interacting gene across all treatment groups and timepoints within a genotype. Once data were appropriately scaled, ToxPi visualizations were generated using ToxPi software (<https://toxpi.org/>; v2.3).

Upstream regulator prediction analyses

Ingenuity Pathway Analysis (IPA, v. 01-22-01; Qiagen Bioinformatics, Redwood City, California) was used to identify predicted upstream regulators associated with DEGs for each treatment group, timepoint, and mouse genotype. Fold change and statistical values determined by DESeq2 were used to conduct the analyses, specifically DEGs with FDR <10%.

Benchmark concentration analyses

BMDEExpress software (v2.3) (Phillips et al., 2019) was used to perform concentration-response modeling to identify genes altered by chemical treatment in mouse hepatocytes according to the methods described in the companion publication (Heintz et al., 2024). Concentration-responsive genes with a best benchmark concentration (BMC) >10-fold below the lowest concentration or a best BMC>the highest concentration were removed (NTP, 2018). Functional classification of significantly concentration-responsive genes (ie, genes with a winning model fit *p*-value \geq .1) was conducted using the Reactome gene set collections available within the BMDEExpress software. Genes were removed according to the default parameters as follows: genes with BMC/BMCL >20, BMCU/BMC >20, and BMCU/BMCL >40 (NTP, 2018). No filters for minimum or maximum number of genes per gene set were applied. BMCs for the gene sets were also calculated.

Results

Transcriptomic changes associated with treatment in WT and PPAR KO mouse hepatocytes

Using the criteria described in the Materials and Methods section for the assessment of sequencing data quality, 7 samples were removed from the analysis for WT mouse hepatocytes and 10 samples were removed for PPAR α KO mouse hepatocytes. Final sample numbers for each treatment group included in downstream transcriptomic analyses are provided in [Supplementary Table 1](#) and [Supplementary File 1](#). In general, samples removed across mouse genotypes were from different chemical treatment groups and timepoints; however, at 72 h, all three 10 mM (highest concentration tested) samples for acetaminophen in WT and PPAR α KO hepatocytes did not meet sequencing data quality criteria and were removed from the analysis. Findings regarding poor sequencing data quality in the 10-mM acetaminophen treatment group at 72 h for both WT and PPAR α KO hepatocytes are consistent with cytotoxicity results (available in [Supplementary File 2](#) and [Supplementary Figure 1](#)). In addition, at 12 h, 2 of the 3 total samples from the 1-mM acetaminophen treatment group in PPAR α KO hepatocytes did not meet sequencing data quality criteria, as a result, this treatment group was also removed from the analysis. Cytotoxicity was primarily observed in hepatocytes treated with acetaminophen or d-galactosamine, the positive controls for a cytotoxic MOA. As expected, cytotoxicity increased with exposure duration (ie, later timepoints, 24 and 72 h) and

concentration (ie, 3 and 10 mM) for acetaminophen and d-galactosamine across hepatocyte genotypes ([Supplementary File 2](#) and [Supplementary Figure 1](#)).

The variance in transcriptomic profiles between each sample across chemical treatment groups and timepoints in WT or PPAR α KO hepatocytes was visualized using principal component analysis (PCA) ([Supplementary Figs. 2–4](#)). PCA results were consistent with findings in the companion publication (Heintz et al., 2024), with the greatest variance attributed to treatment duration (ie, timepoint). Chemical treatment group also contributed to the observed variation between samples, with acetaminophen and d-galactosamine-treated samples having the greatest separation from the other chemical groups in both WT and PPAR α KO hepatocytes, particularly at 24 and 72 h timepoints ([Supplementary Figure 3](#)). Samples from HFPO-DA, GW7647, and rosiglitazone treatment groups clustered more closely with solvent control samples within each timepoint; however, upon removal of samples treated with acetaminophen and d-galactosamine, HFPO-DA and GW7647-treated samples from WT hepatocytes generally clustered together and separately from rosiglitazone and control samples at 12 and 24 h ([Supplementary Figure 4](#)). A distinct clustering pattern following removal of samples treated with acetaminophen and d-galactosamine was not observed in samples from WT hepatocytes at 72 h or in samples from PPAR α KO hepatocytes. PCA results were consistent with hierarchical clustering patterns observed within each hepatocyte genotype ([Supplementary Figs. 5A and B](#)); in addition, as expected, samples generally grouped by hepatocyte genotype followed by timepoint when all samples were analyzed together by hierarchical clustering ([Supplementary Figure 5C](#)).

The number of significantly upregulated DEPs across timepoints for each chemical treatment group in WT and PPAR α KO hepatocytes are presented in [Figure 2](#) (results for downregulated DEPs available in [Supplementary Figure 6](#); also available in [Supplementary File 3](#)). Consistent with results presented in the companion publication (Heintz et al., 2024), hepatocytes treated with acetaminophen and d-galactosamine generally had the greatest number of DEPs at each timepoint compared with the other chemicals tested.

Across timepoints, the number of DEPs was comparable for HFPO-DA and GW7647, and to a lesser extent rosiglitazone, in WT hepatocytes. In PPAR α KO hepatocytes, the number of DEPs was more variable between HFPO-DA, GW7647, and rosiglitazone. At 12 h, rosiglitazone exhibited a high number of DEPs, whereas HFPO-DA and GW7647 had a low number of DEPs. At 24 h, a greater number of DEPs were observed in HFPO-DA-treated PPAR α KO hepatocytes than GW7647 or rosiglitazone counterparts; however, by 72 h, the number of DEPs was comparable between all 3 chemicals.

When comparing across genotypes, at 12 h, fewer significantly altered DEPs were observed in both HFPO-DA and GW7647-treated PPAR α KO hepatocytes compared with WT counterparts. Conversely, rosiglitazone had a comparable number of DEPs between hepatocyte genotypes at 12 h. At 24 h, there were more DEPs in PPAR α KO hepatocytes exposed to HFPO-DA than WT hepatocytes. A comparable number of probes were differentially expressed between genotypes in GW7647 and rosiglitazone-treated hepatocytes at 24 h, and by 72 h, a lower number of DEPs were observed for all 3 chemicals in PPAR α KO hepatocytes compared with WT counterparts.

Overall, treatment duration had the greatest impact on variance in transcriptomic profiles between hepatocyte samples for both WT and PPAR α KO hepatocytes. Mouse hepatocytes treated with acetaminophen or d-galactosamine generally had a

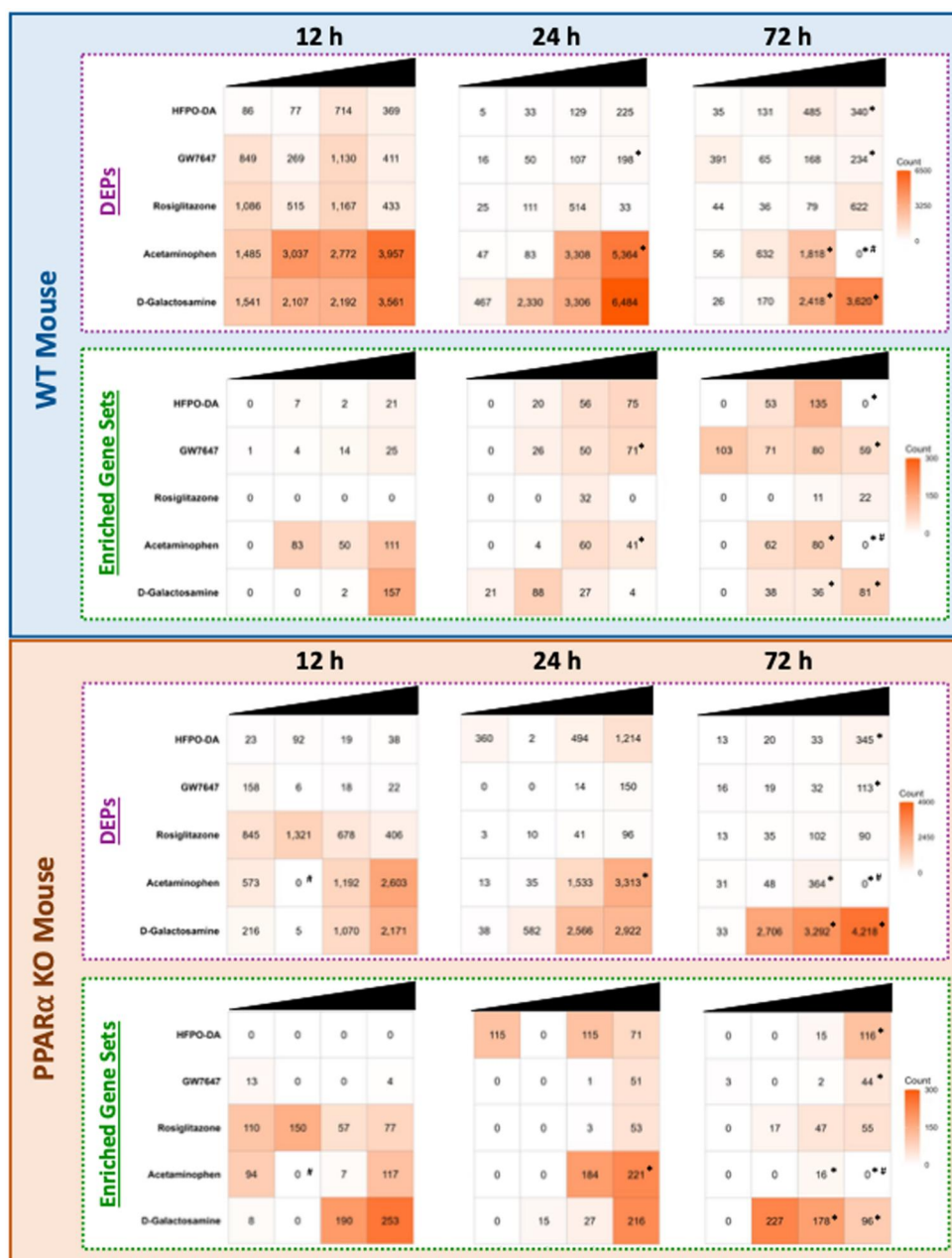


Figure 2. Number of significantly upregulated DEPs (FDR<10%) and enriched gene sets (FDR<5%) for each chemical tested (relative to controls) in WT and PPAR α KO mouse hepatocytes across 12, 24, and 72 h. Each row represents a different chemical and each column represents a different test concentration, with concentrations increasing from left to right. An “*” indicates that cytotoxicity was observed at this concentration and timepoint. An “#” indicates that samples from this concentration and timepoint did not undergo transcriptomic analyses due to low sequencing quality.

different and greater transcriptomic response based on PCA and total differential gene expression counts compared with the other chemicals tested. In addition, a difference in the number of DEPs between genotypes was observed at the early timepoints for HFPO-DA and GW7647-treated hepatocytes.

Comparison of pathway-level responses to HFPO-DA and positive controls in WT and PPAR α KO mouse hepatocytes

The number of significant (FDR<5%) upregulated gene sets differed between WT and PPAR α KO hepatocytes that received the same treatment, particularly at the 12-h timepoint for HFPO-DA, GW7647, and rosiglitazone-treated hepatocytes (Figure 2, Tables 1–3; Supplementary File 4). In WT hepatocytes, the

number of significantly upregulated gene sets increased with increasing concentration for both HFPO-DA and GW7647 across timepoints, apart from 72 h, where changes in hepatocyte morphology and LDH release, indicative of cell death, were observed at the highest concentrations. Enriched gene sets were similar between the 2 chemicals across timepoints and related to β -oxidation of fatty acids and PPAR signaling (see Tables 1–3). Conversely, in PPAR α KO hepatocytes at 12 h, zero gene sets were upregulated following HFPO-DA treatment, and only a few gene sets were upregulated in the lowest and highest concentration groups for GW7647. The 13 enriched gene sets in the lowest concentration group for GW7647 (0.01 μ M) were specifically related to mitochondrial stress, whereas the 4 gene sets upregulated in

Table 1. Top 5 most significant upregulated gene sets across treatment concentrations at 12 h in WT and PPAR α KO mouse hepatocytes

Chemical	WT			PPAR α KO		
	Concentration	Upregulated gene set	Adjusted p-value	Concentration	Upregulated gene set	Adjusted p-value
HFPO-DA	500 μ M	KEGG fatty acid metabolism	8.38E-10	NS	NS	NS
	500 μ M	WP fatty acid β -oxidation	1.72E-08			
	500 μ M	WP mitochondrial long-chain fatty acid β -oxidation	2.28E-07			
GW7647	500 μ M	REACTOME fatty acid metabolism	3.92E-07			
	10 μ M	KEGG PPAR Signaling Pathway	2.13E-06	0.01 μ M	KEGG Alzheimer's Disease	.0002597
	10 μ M	WP fatty acid β -oxidation	7.83E-11	0.01 μ M	KEGG Oxidative Phosphorylation	.001082
	10 μ M	REACTOME fatty acid metabolism	8.26E-11			
	10 μ M	WP PPAR signaling pathway	1.92E-09	0.01 μ M	REACTOME Respiratory Electron Transport ATP Synthesis by Chemiosmotic Coupling and Heat Production by Uncoupling Proteins	.001082
Rosiglitazone	10 μ M	KEGG PPAR signaling pathway	2.28E-09	0.01 μ M	WP Electron Transport Chain Oxidative Phosphorylation System in Mitochondria	.001238
	10 μ M	WP mitochondrial long-chain fatty acid β -oxidation	4.30E-09	10 μ M	WP Mitochondrial Long-Chain Fatty Acid β -oxidation	.004178
	NS	NS	NS	0.1 μ M	REACTOME Translation	1.61E-15
				0.01 μ M	REACTOME Regulation of Expression of SLITS and ROBOS	7.00E-11
				0.01 μ M	REACTOME Translation	7.00E-11
Acetaminophen	10 mM	REACTOME Regulation of Expression of SLITS and ROBOS	1.63E-09	0.1 μ M	REACTOME Regulation of Expression of SLITS and ROBOS	1.63E-09
	10 mM	REACTOME Signaling of ROBO Receptors	1.91E-09	0.01 μ M	REACTOME Signaling of ROBO Receptors	1.91E-09
	10 mM	REACTOME Cellular Response to Starvation	2.95E-27	10 mM	REACTOME Cellular Response to Starvation	2.95E-27
	10 mM	REACTOME Response of EIF2AK4 (GCN2) to Amino Acid Deficiency	2.95E-27	10 mM	REACTOME Response of EIF2AK4 (GCN2) to Amino Acid Deficiency	2.95E-27
	10 mM	REACTOME Eukaryotic Translation Initiation	1.18E-26	10 mM	REACTOME Eukaryotic Translation Initiation	1.18E-26
D-Galactosamine	10 mM	REACTOME Eukaryotic Translation Elongation	4.01E-25	10 mM	REACTOME Eukaryotic Translation Elongation	4.01E-25
	1 mM	REACTOME Nonsense Mediated Decay	2.42E-23	10 mM	REACTOME Nonsense Mediated Decay	2.42E-23
	10 mM	REACTOME Translation	1.12E-15	10 mM	REACTOME Translation	1.12E-15
	10 mM	REACTOME Eukaryotic Translation Initiation	4.45E-14	10 mM	REACTOME Eukaryotic Translation Initiation	4.45E-14
	10 mM	REACTOME Metabolism of Amino Acids and Derivatives	1.05E-13	10 mM	REACTOME Metabolism of Amino Acids and Derivatives	1.05E-13
D-Galactosamine	10 mM	WP VEGF-A/VEGFR-2 Signaling Pathway	3.32E-12	10 mM	WP VEGF-A/VEGFR-2 Signaling Pathway	3.32E-12
	10 mM	REACTOME eukaryotic translation initiation	8.50E-10	10 mM	REACTOME eukaryotic translation initiation	8.50E-10
	10 mM	REACTOME eukaryotic translation elongation	1.09E-09	10 mM	REACTOME Selenoamino Acid Metabolism	4.02E-11

Abbreviations: NS, not significant, ie, gene sets did not meet significance threshold (adjusted p -value < .05) for gene set enrichment.

the highest concentration group (10 μ M) were related to mitochondrial fatty acid β -oxidation. Responses observed in the lowest concentration group for GW7647 at 12 h may be indicative of a mitohormetic response, because responses at higher concentrations and later timepoints did not include a mitochondrial stress response and were instead related to PPAR α signaling and mitochondrial β -oxidation (Cox et al., 2018). Regardless of the types of enriched gene sets, the adjusted p -values for all enriched gene sets in GW7647-treated PPAR α KO hepatocytes at 12 h were at least 6-fold greater (ie, 6-fold lower significance) than adjusted p -values for upregulated gene sets in WT counterparts, indicating a lower transcriptomic response (Table 1).

At later timepoints (ie, 24 and 72 h), significantly upregulated gene sets for HFPO-DA and GW7647-treated PPAR α KO hepatocytes were generally limited to the 2 highest concentration groups. The types of gene sets significantly upregulated by both chemicals in PPAR α KO hepatocytes were similar to WT hepatocytes treated with HFPO-DA or GW7647, and were related to PPAR signaling and fatty acid metabolism/ β -oxidation (Tables 2 and 3). However, in the lowest concentration group for HFPO-DA-treated PPAR α KO hepatocytes at 24 h, genes underlying significantly upregulated gene sets were largely related to protein ubiquitination (eg, *Psma*, *Psmc*, *Psmd*, *Psme*) (Table 2; Supplementary File 4). This response was not observed at higher concentrations or at 72 h.

Table 2. Top 5 most significant upregulated gene sets across treatment concentrations at 24 h in WT and PPAR α KO mouse hepatocytes

Chemical	WT			PPAR α KO		
	Concentration	Upregulated gene set	Adjusted p-value	Concentration	Upregulated gene set	Adjusted p-value
HFPO-DA	500 μ M	KEGG fatty acid metabolism	1.10E-26	500 μ M	KEGG Fatty Acid Metabolism	5.79E-10
	50 μ M	REACTOME fatty acid metabolism	4.36E-22	50 μ M	KEGG Fatty Acid Metabolism	8.74E-08
	500 μ M	REACTOME fatty acid metabolism	4.82E-22	50 μ M	REACTOME Fatty Acid Metabolism	3.57E-07
	500 μ M	KEGG fatty acid metabolism	5.83E-20	50 μ M	REACTOME Metabolism of Amino Acids and Derivatives	9.67E-07
	500 μ M	KEGG PPAR signaling pathways	2.50E-15	0.1 μ M	REACTOME ABC Transporter Disorders	4.57E-06
GW7647	10 μ M	KEGG fatty acid metabolism	7.55E-30	10 μ M	REACTOME Fatty Acid Metabolism	5.44E-20
	10 μ M	REACTOME fatty acid metabolism	1.50E-23	10 μ M	KEGG PPAR Signaling Pathways	3.55E-14
	10 μ M	KEGG PPAR signaling pathway	5.40E-21	10 μ M	WP PPAR Signaling Pathways	5.27E-13
	10 μ M	WP PPAR signaling pathway	9.31E-20	10 μ M	KEGG Fatty Acid Metabolism	4.05E-11
	1 μ M	KEGG fatty acid metabolism	6.72E-15	10 μ M	KEGG Peroxisome	2.04E-09
Rosiglitazone	1 μ M	REACTOME regulation of IFNA/B signaling	8.02E-15	10 μ M	REACTOME Fatty Acid Metabolism	8.78E-18
	1 μ M	WP SARS coronavirus and innate immunity	1.40E-13	10 μ M	KEGG PPAR Signaling Pathway	7.30E-15
	1 μ M	REACTOME TRAF6 mediated IRF7 activation	5.24E-11	10 μ M	WP_PPAR Signaling Pathway	1.98E-13
	1 μ M	WP overview of interferons mediated signaling pathway	5.24E-11	10 μ M	REACTOME Peroxisomal Lipid Metabolism	4.63E-10
	1 μ M	REACTOME interferon alpha/beta signaling	5.35E-11	10 μ M	REACTOME Peroxisomal Protein Import	6.22E-09
Acetaminophen	10 mM	REACTOME cellular response to starvation	4.50E-07	10 mM	REACTOME Regulation of Expression of SLITs and ROBOs	2.47E-27
	10 mM	REACTOME response of EIF2AK4 (GCN2) to amino acid deficiency	4.50E-07	10 mM	REACTOME Nonsense Mediated Decay (NMD)	1.51E-24
	10 mM	REACTOME eukaryotic translation elongation	8.06E-07	10 mM	REACTOME Influenza Infection	8.56E-24
	10 mM	REACTOME nonsense mediated decay (NMD)	8.51E-07	10 mM	REACTOME Cellular Response to Starvation	3.18E-23
	10 mM	REACTOME eukaryotic translation initiation	1.17E-06	10 mM	REACTOME Eukaryotic Translation Elongation	3.18E-23
D-Galactosamine	0.3 mM	REACTOME metabolism of amino acid and derivatives	2.82E-07	10 mM	REACTOME Translation	4.77E-45
	1 mM	REACTOME eukaryotic translation initiation	1.23E-05	10 mM	REACTOME Eukaryotic Translation Initiation	7.64E-31
	3 mM	REACTOME TRAF6 mediated IRF7 activation	1.26E-05	10 mM	REACTOME Eukaryotic Translation Elongation	2.69E-27
	1 mM	REACTOME regulation of expression of SLITs and ROBOs	2.02E-05	10 mM	REACTOME Regulation of Expression of SLITs and ROBOs	5.40E-26
	0.3 mM	KEGG ribosome	2.09E-05	10 mM	KEGG Ribosome	1.28E-25

The apparent initial temporal delay in transcriptomic response to HFPO-DA and GW7647 treatment in PPAR α KO hepatocytes at 12 h was not observed in PPAR α KO hepatocytes treated with rosiglitazone, acetaminophen, or d-galactosamine. In contrast to the PPAR α activators, the PPAR γ agonist rosiglitazone increased pathway enrichment across treatment groups at 12 h in PPAR α KO hepatocytes but not in WT hepatocytes (Figure 2, Table 1). At higher concentrations and later timepoints, the types of upregulated gene sets in rosiglitazone-treated hepatocytes, especially PPAR α KO, were similar to enriched gene sets in HFPO-DA and GW7647-treated hepatocytes and related to PPAR signaling and fatty acid metabolism (see Tables 2 and 3). However, the genes underlying these gene sets are regulated by multiple nuclear receptors involved in maintaining energy homeostasis. For example, the “KEGG PPAR Signaling Pathway” consists of 3 PPAR isoforms ($\alpha/\delta/\gamma$)

and while specific genes are regulated by specific receptors, there is also substantial overlap in regulation, with several genes regulated by all 3 PPAR isoforms (Chappell et al., 2020; Heintz et al., 2022).

In general, the number of significantly enriched gene sets in acetaminophen and d-galactosamine treatment groups was greater in PPAR α KO hepatocytes across all timepoints, however, the types of gene sets enriched for each chemical were consistent between mouse genotypes and appeared to be unrelated to fatty acid metabolism or energy homeostasis (Tables 1–3; Supplementary File 4). Fewer gene sets were significantly downregulated (compared with the number upregulated) across timepoints and chemical treatment groups in both hepatocyte genotypes (Supplementary Figure 6).

Concordance of transcriptomic responses at the pathway level between HFPO-DA and other positive controls was assessed in

Table 3. Top 5 most significant upregulated gene sets across treatment concentrations at 72 h in WT and PPAR α KO mouse hepatocytes

Chemical	WT			PPAR α KO		
	Concentration	Upregulated gene set	Adjusted p-value	Concentration	Upregulated gene set	Adjusted p-value
HFPO-DA	50 μ M	KEGG fatty acid metabolism	4.18E-23	500 μ M	REACTOME Fatty Acid Metabolism	4.38E-17
	500 μ M	REACTOME fatty acid metabolism	4.55E-22	500 μ M	KEGG Fatty Acid Metabolism	5.00E-15
	5 μ M	KEGG fatty acid metabolism	5.22E-21	500 μ M	REACTOME Phase I Functionalization of Compounds	1.35E-10
	5 μ M	REACTOME fatty acid metabolism	7.48E-17	500 μ M	KEGG PPAR Signaling Pathway	2.80E-10
	5 μ M	KEGG PPAR signaling pathway	5.59E-16	500 μ M	REACTOME Biological Oxidations	2.80E-10
GW7647	10 μ M	KEGG fatty acid metabolism	4.85E-27	10 μ M	KEGG PPAR Signaling Pathway	2.73E-16
	1 μ M	KEGG fatty acid metabolism	8.01E-26	10 μ M	WP PPAR Signaling Pathway	4.57E-15
	0.01 μ M	REACTOME fatty acid metabolism	2.02E-25	10 μ M	REACTOME Fatty Acid Metabolism	2.33E-14
	1 μ M	REACTOM fatty acid metabolism	8.78E-24	10 μ M	KEGG Fatty Acid Metabolism	4.61E-11
Rosiglitazone	0.01 μ M	KEGG fatty acid metabolism	7.85E-23	10 μ M	WP Fatty Acid Transporters	5.01E-09
	1 μ M	KEGG PPAR signaling pathway	6.65E-05	10 μ M	KEGG PPAR Signaling Pathway	3.89E-16
	1 μ M	WP PPAR α pathway	6.65E-05	10 μ M	REACTOME Fatty Acid Metabolism	3.89E-16
	1 μ M	WP PPAR signaling pathway	6.65E-05	10 μ M	WP PPAR Signaling Pathway	6.17E-15
Acetaminophen	10 μ M	REACTOME protein localization	1.63E-04	1 μ M	KEGG PPAR Signaling Pathway	6.59E-12
	3 mM	REACTOME metabolism of amino acids and derivatives	2.30E-10	3 mM	WP NRF2 Pathway	2.60E-04
	1 mM	REACTOME metabolism of amino acids and derivatives	2.96E-10	3 mM	REACTOME HSF1 Dependent Transactivation	5.04E-04
	3 mM	WP metabolic reprogramming in colon cancer	1.48E-09	3 mM	WP Ferroptosis	5.04E-04
	1 mM	WP amino acid metabolism	1.36E-08	3 mM	REACTOME Attenuation Phase	5.70E-04
	1 mM	KEGG drug metabolism cytochrome P450	1.00E-07	3 mM	REACTOME HSF1 Activation	9.64E-04
	D-Galactosamine	1 mM	WP NRF2 pathway	2.22E-11	1 mM	REACTOME rRNA Processing
3 mM		REACTOME rRNA processing	3.34E-10	3 mM	REACTOME rRNA Processing	6.01E-30
10 mM		REACTOME rRNA processing	1.48E-08	10 mM	REACTOME rRNA Processing	1.53E-27
3 mM		REACTOME rRNA modification in the nucleus and cytosol	1.98E-08	10 mM	REACTOME Eukaryotic Translation Elongation	2.95E-26
3 mM		REACTOME chromatin modifying enzymes	2.20E-08	10 mM	REACTOME Eukaryotic Translation Initiation	2.95E-26

WT and PPAR α KO hepatocytes by aggregating gene sets according to known chemical–gene interactions. Gene set aggregation visuals (ie, ToxPi visuals, PCA plots) for WT hepatocytes were consistent with results observed in hepatocytes from other WT rodent species and strains (see companion publication; Heintz *et al.*, 2024), and demonstrated homogeneous upregulated gene set enrichment profiles for HFPO-DA and GW7647 (ie, similar ToxPi wedge pattern and size across treatment concentrations and timepoints, and greater overlap in PCA plots) using both internal (within a specific chemical treatment group, timepoint, and genotype) and external (across chemical treatment groups and timepoints within a specific genotype) scaling approaches (described in the Materials and Methods section) (Figs. 3 and 4; Supplementary Figure 7). HFPO-DA also had the greatest concordance with GW7647 in PPAR α KO hepatocytes by both internal and external scaling approaches.

At higher concentrations and later timepoints, upregulated gene set enrichment profiles for rosiglitazone were more similar to HFPO-DA and GW7647 in PPAR α KO hepatocytes, especially when the external scaling approach was used (Figs. 3 and 4). For both hepatocyte genotypes, upregulated gene set enrichment profiles for

acetaminophen and d-galactosamine-treated hepatocytes were most concordant with each other (Figure 4); in addition, each cytotoxic agent demonstrated similar ToxPi profile patterns between WT and PPAR α KO hepatocytes (Figure 3; Supplementary Figure 7). Due to the lower number of significant downregulated gene sets in WT and PPAR α KO hepatocytes across chemical treatment groups and timepoints (Supplementary Figure 6), aggregation analyses of downregulated gene sets were not able to be performed.

Overall, compared with WT hepatocytes, initial transcriptomic responses at the pathway-level were delayed in PPAR α KO hepatocytes treated with HFPO-DA or GW7647, as little to no significant gene set enrichment was observed at 12 h for either chemical. This initial temporal delay in transcriptomic response was not observed in rosiglitazone, acetaminophen, or d-galactosamine-treated PPAR α KO hepatocytes. At later time points and higher concentrations, ToxPi profiles demonstrated greatest pathway level concordance between HFPO-DA and GW7647-treated hepatocytes in both WT and PPAR α KO hepatocytes. In addition, rosiglitazone treatment in PPAR α KO hepatocytes resulted in more similar ToxPi profiles to that of HFPO-DA and GW7647 treatment, especially at 24 and 72 h.

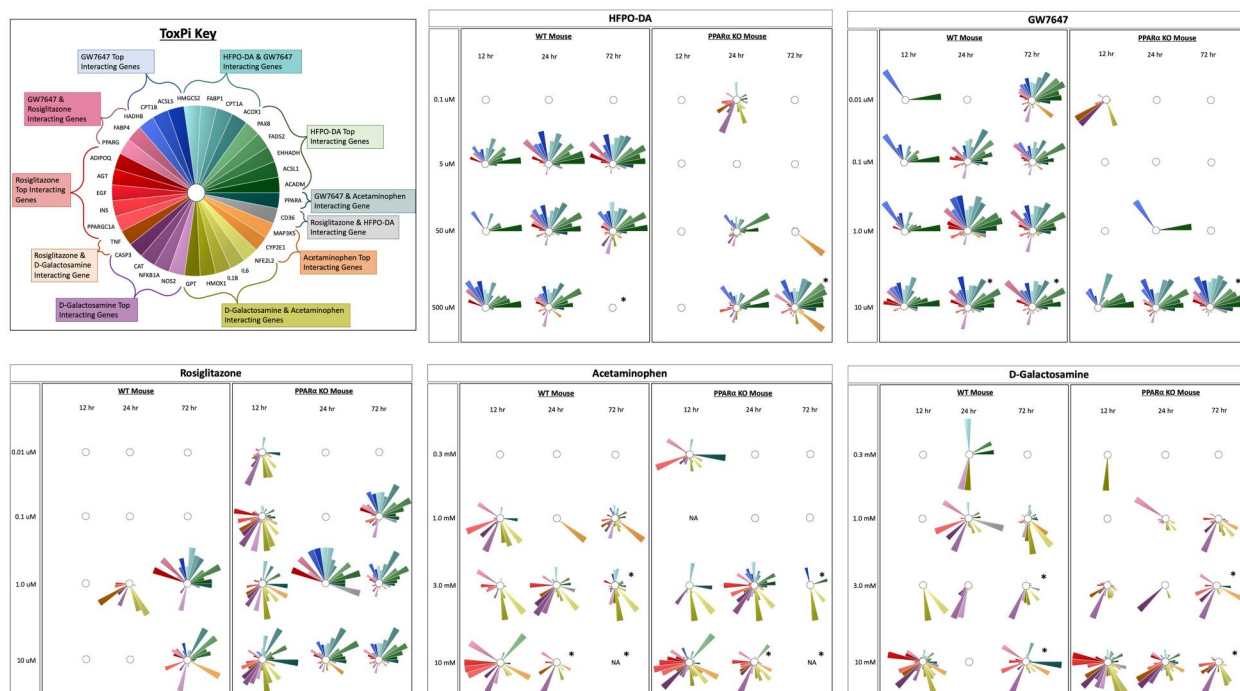


Figure 3. ToxPi visualizations of upregulated gene set aggregation results for WT and PPAR α KO mouse hepatocytes using internal scaling approach. Significant (FDR < 5%) upregulated gene sets from hypergeometric gene set enrichment analysis containing genes known to interact with HFPO-DA and/or positive controls were aggregated as described in the Materials and Methods section. The size of a ToxPi wedge for a given gene reflects the significance and number of enriched gene sets containing that gene within a specific chemical treatment group and timepoint that is scaled in respect to the other wedges for different genes within the same ToxPi (ie, internal scaling). An “*” indicates that cytotoxicity was observed at this concentration and timepoint. An empty ToxPi indicates that none of the targeted gene sets were enriched significantly, and “NA” means that samples from this concentration and timepoint did not undergo transcriptomic analyses due to low sequencing quality.

Comparison of upstream regulator predictions across chemical treatment groups in WT and PPAR α KO mouse hepatocytes

The top 20 predicted upstream regulators for HFPO-DA-treated WT and PPAR α KO hepatocytes were identified using QIAGEN Ingenuity Pathway Analysis (IPA) for each timepoint. The activation/inhibition z-scores for each of these 20 predicted upstream regulators were then compared across chemical treatment groups for each timepoint and hepatocyte genotype (Figure 5). Similar activation/inhibition patterns between HFPO-DA and GW7647 were observed across all 3 timepoints in WT hepatocytes. At 12 h, rosiglitazone-treated WT hepatocytes shared a somewhat consistent predicted upstream regulator pattern to HFPO-DA and GW7647 counterparts. However, by 24 and 72 h, predicted regulator patterns for rosiglitazone were consistent, albeit substantially weaker, than predicted regulator patterns for HFPO-DA and GW7647 in WT hepatocytes. In contrast, patterns of predicted upstream regulator activation/inhibition for acetaminophen and d-galactosamine were generally inconsistent with predicted regulator activation/inhibition patterns for HFPO-DA in WT hepatocytes.

Due to the limited transcriptomic response at earlier timepoints (see Figs. 2 and 3), upstream regulator predictions were reduced for HFPO-DA and GW7647-treated PPAR α KO hepatocytes, especially at 12 h (Figure 5). Consistency in upstream regulator prediction patterns between HFPO-DA, GW7647, and rosiglitazone increased across time in PPAR α KO hepatocytes. In addition, similar to what was observed in WT hepatocytes, predicted regulator activation/inhibition patterns for acetaminophen and d-galactosamine-treated PPAR α KO hepatocytes were inconsistent with patterns observed in HFPO-DA counterparts.

PPAR α was the top predicted upstream regulator in WT hepatocytes treated with HFPO-DA or GW7647 across all 3 timepoints (Figure 5; Supplementary Figs. 8–10). PPAR α was also the top predicted upstream regulator in PPAR α KO hepatocytes at 12 and 72 h for these 2 chemicals (Supplementary Figs. 8 and 10). In addition, PPAR α was also predicted as the top regulator for the prototypical PPAR γ agonist rosiglitazone at 72 h in PPAR α KO hepatocytes (Supplementary Figure 10), which is consistent with gene set enrichment analysis results shown in Table 3.

Overall, upstream regulator prediction patterns for HFPO-DA are most similar to GW7647 in both hepatocyte genotypes, however, at earlier timepoints, regulator predictions for HFPO-DA and GW7647-treated PPAR α KO hepatocytes were limited due to a lower number of DEPs. At 72 h, regulator prediction patterns for HFPO-DA and GW7647 were also similar to regulator prediction patterns for rosiglitazone.

Benchmark concentration modeling of gene expression data from WT and PPAR α KO mouse hepatocytes

The concentration-response across all genes for each treatment group and timepoint in WT and PPAR α KO hepatocytes was modeled using BMDEpress v2.3 (Phillips et al., 2019) (Supplementary File 5). As shown in Figure 6, there were comparable patterns in BMC values for concentration-response genes in WT and PPAR α KO hepatocytes for each of the chemical treatments except for rosiglitazone, where treated WT hepatocytes had a greater number of genes with a best BMC between 0.1 and 10 μ M than PPAR α KO counterparts. Also highlighted in Figure 6 are the BMC values for various PPAR α responsive genes and CYPs involved in lipid metabolism across hepatocyte genotypes and chemical treatment groups at 24 h (results for 12 and 72 h shown in

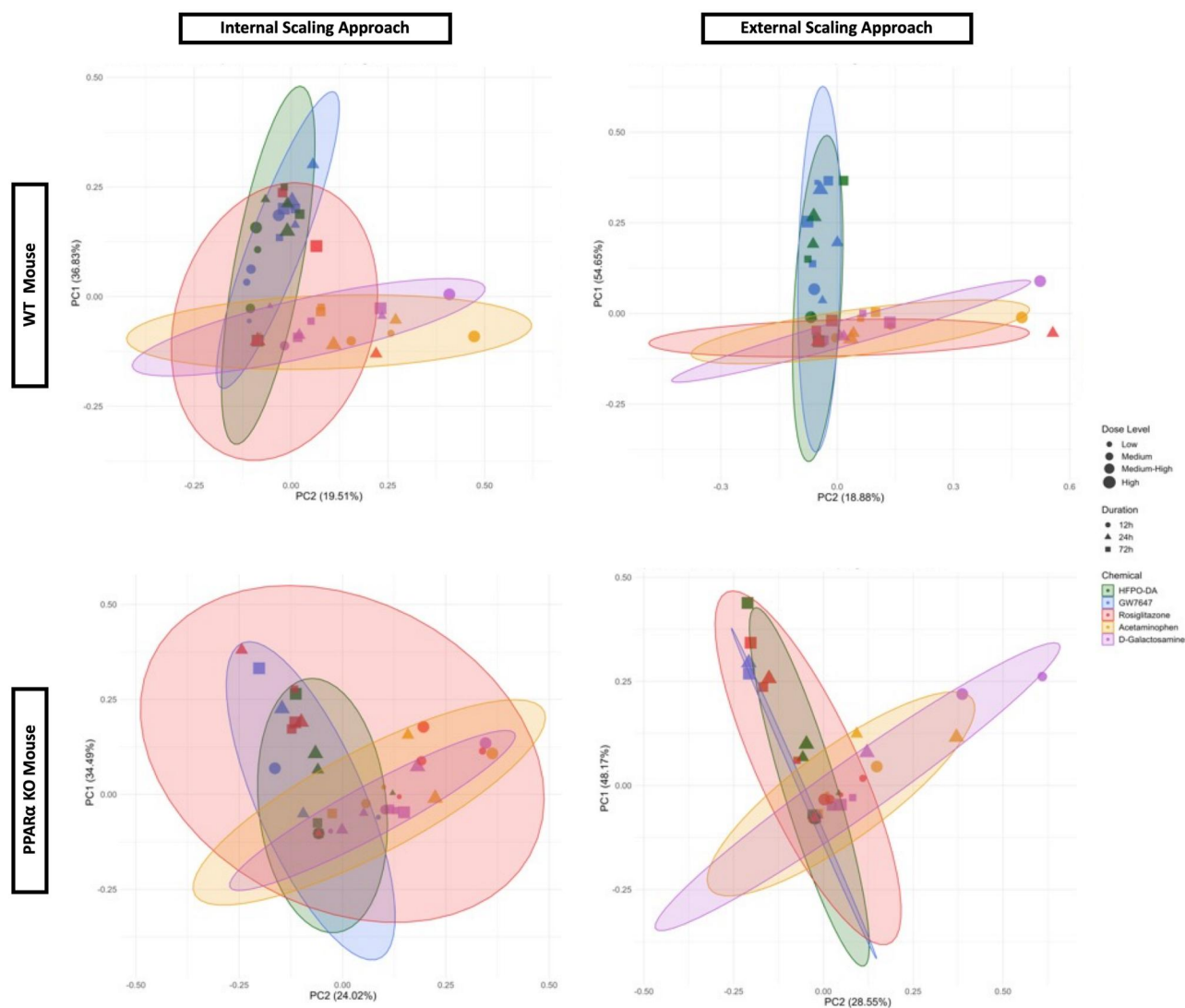


Figure 4. PCA of upregulated gene set aggregation results for WT and PPAR α KO mouse hepatocytes using internal and external scaling methods. Shaded ellipses are based on the covariance matrix of the aggregated gene set results with ellipse size accounting for aspects of the underlying cumulative probability distribution, ie, the ellipses provide general insight into the directionality and variance of the respective chemical treatment groups.

Supplementary Figs. 11 and 12). The BMC values for PPAR α target genes were consistently lower than the BMC values for lipid metabolizing CYPs in WT hepatocytes treated with HFPO-DA or GW7647. This was also observed in WT mouse, rat, and human hepatocytes treated with either HFPO-DA or GW7647 (see companion publication). In contrast, the BMC values for PPAR α target genes in PPAR α KO hepatocytes treated with HFPO-DA or GW7647 were consistently higher (ie, approximately 10-fold greater) than the BMC values in WT counterparts across timepoints (Figs. 6 and 7; Supplementary Figs. 11–13). For example, at 24 h, the lowest BMCs for PPAR α target genes in WT hepatocytes were approximately 1.3 and approximately 0.013 μ M, for HFPO-DA and GW7647, respectively; whereas, in PPAR α KO hepatocytes, the lowest BMCs for PPAR α target genes were approximately 14 and approximately 0.1 μ M, for HFPO-DA and GW7647, respectively (Figure 7). These results indicate a shift in the activation concentration of PPAR α target genes in PPAR α KO hepatocytes treated with HFPO-DA or GW7647. This shift in the activation of PPAR α target genes was not observed in PPAR α

KO hepatocytes treated with rosiglitazone, acetaminophen, or d-galactosamine at any timepoint.

Similar to PPAR α target genes, median BMCs for PPAR α -related signaling pathways (ie, fatty acid metabolism/ β -oxidation) were also approximately 10-fold higher in HFPO-DA-treated PPAR α KO hepatocytes compared with WT counterparts at 24 h (Figure 8; Supplementary File 6). For example, out of the top 6 most significantly enriched signaling pathways among concentration-responsive genes in HFPO-DA-treated WT and PPAR α KO hepatocytes at 24 h, most signaling pathways were related to fatty acid metabolism or peroxisomal proteins, with 5 out of the 6 pathways shared between genotypes. From these top significantly enriched pathways, median BMCs ranged from 3.3 to 4.6 μ M and 31 to 32 μ M for HFPO-DA-treated WT and PPAR α KO hepatocytes, respectively (Figure 8). This comparison of signaling pathway enrichment among concentration-responsive genes between HFPO-DA-treated WT and PPAR α KO hepatocytes was not possible at the 12- or 72-h timepoints due to the low number of concentration-responsive genes in WT and/or PPAR α KO

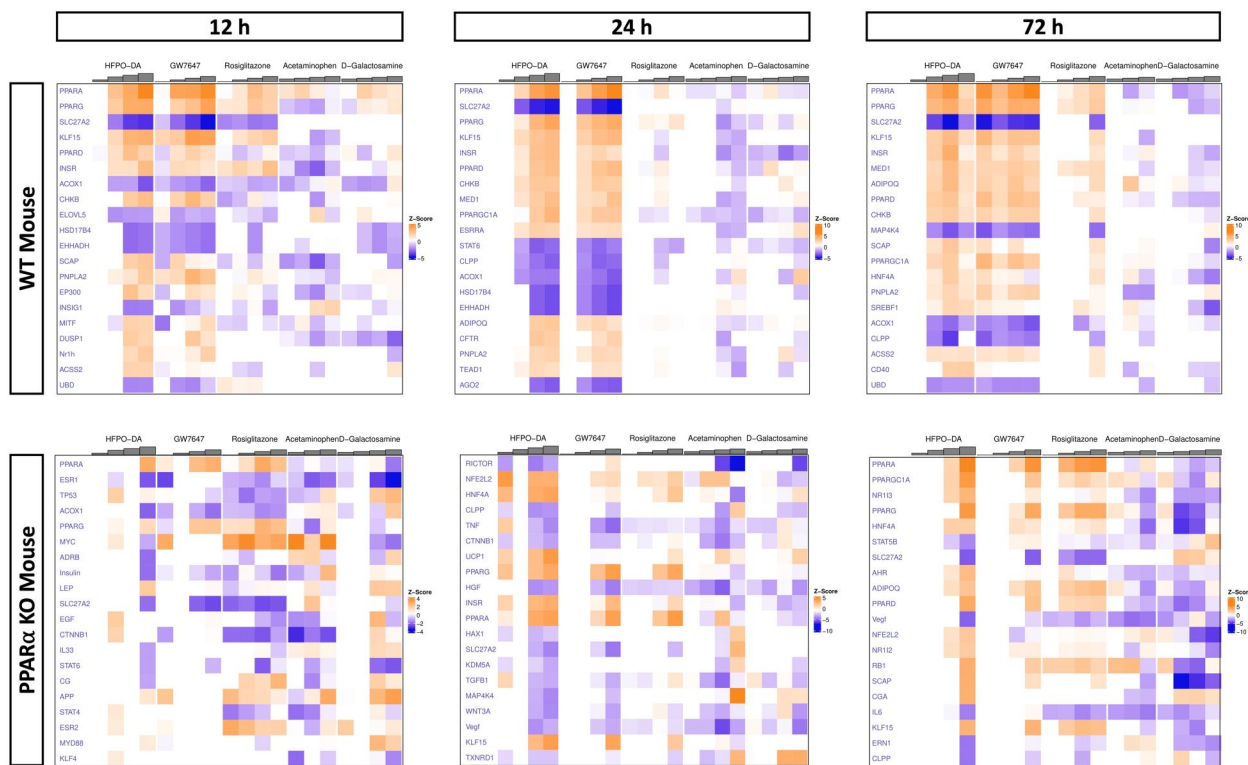


Figure 5. Comparison of activation/inhibition patterns for HFPO-DA's top 20 predicted upstream regulators across chemical treatment groups at 12, 24, and 72 h. Each column represents a different test concentration, with concentrations increasing from left to right for each chemical. Orange indicates predicted activation, and blue indicates predicted inhibition; the intensity of each color increases with the absolute z-score. Columns with no z-score prediction indicate chemical treatment groups with a low number DEGs and upstream regulator predictions were not able to be estimated.

hepatocytes. Among concentration-responsive genes in GW7647-treated hepatocytes at 24 h, there were no significantly enriched (ie, Fisher's exact 2-tail <0.1) signaling pathways in WT hepatocytes, however, the top most significantly enriched pathways in PPAR α KO hepatocytes were also related to fatty acid metabolism or peroxisomal proteins and had median BMCs greater than the second highest concentration tested for GW7647, ranging from approximately 2.2 to approximately 3.8 μM (Supplementary File 6). In contrast, median BMCs for significantly enriched signaling pathways in rosiglitazone, acetaminophen, or d-galactosamine-treated hepatocytes were similar between genotypes (Supplementary File 6).

Overall, consistent with results from gene set enrichment analyses of DEGs using the hypergeometric test, PPAR α -related signaling pathways were among the most significantly enriched pathways for concentration-responsive genes in both WT and PPAR α KO hepatocytes treated with HFPO-DA or GW7647. However, PPAR α target genes and related signaling pathways had approximately 10-fold higher BMCs and median BMCs, respectively, in HFPO-DA and GW7647-treated PPAR α KO hepatocytes compared with WT counterparts. These findings coincide with the observed temporal delay of transcriptomic responses in HFPO-DA and GW7647-treated PPAR α KO hepatocytes.

Discussion

Whole transcriptomic analyses of primary WT and PPAR α KO mouse hepatocytes demonstrated nearly identical transcriptomic signaling pathways and predicted upstream regulators in

both hepatocyte genotypes treated with the short-chain PFAS, HFPO-DA, or the established PPAR α agonist, GW7647. Pathways related to fatty acid metabolism and PPAR signaling were among the most significantly enriched for both of these chemicals. However, responses in PPAR α KO hepatocytes were weaker, and exhibited a distinct temporal and concentration-dependent delay for both chemicals that did not occur in WT hepatocytes. Evidence for this delay was based on a low number of DEPs and general lack of enriched gene sets at 12 h, as well as approximately 10-fold difference between BMCs for PPAR α target genes and associated pathways in WT and PPAR α KO hepatocytes at 24 and 72 h. Conversely, this delay was not observed in PPAR α KO hepatocytes treated with the established PPAR γ agonist, rosiglitazone, or known cytotoxic agents, acetaminophen or d-galactosamine.

The delayed but similar responses in PPAR α KO hepatocytes treated with HFPO-DA or GW7647 to that observed in WT hepatocytes suggest evidence for compensatory mechanisms activated in lieu of PPAR α . Several transcription factors, in addition to PPAR α , control fatty acid homeostasis in the liver including CAR (constitutive androstane receptor), PXR (pregnane X receptor), HNF4 α (hepatocyte nuclear factor 4 alpha), and PPAR δ/γ (Hernandez et al., 2009; Wang et al., 2020). HNF4 α regulates both CAR and PPAR α with the help of the coactivator, PGC-1 α (peroxisome proliferator-activated receptor-gamma coactivator alpha) (Hernandez et al., 2009; Kasano-Camones et al., 2023). Under normal conditions, PPAR α and CAR also compete for PGC-1 α to activate or suppress the beta-oxidation of fatty acids, respectively. However, under certain conditions such as xenobiotic exposure

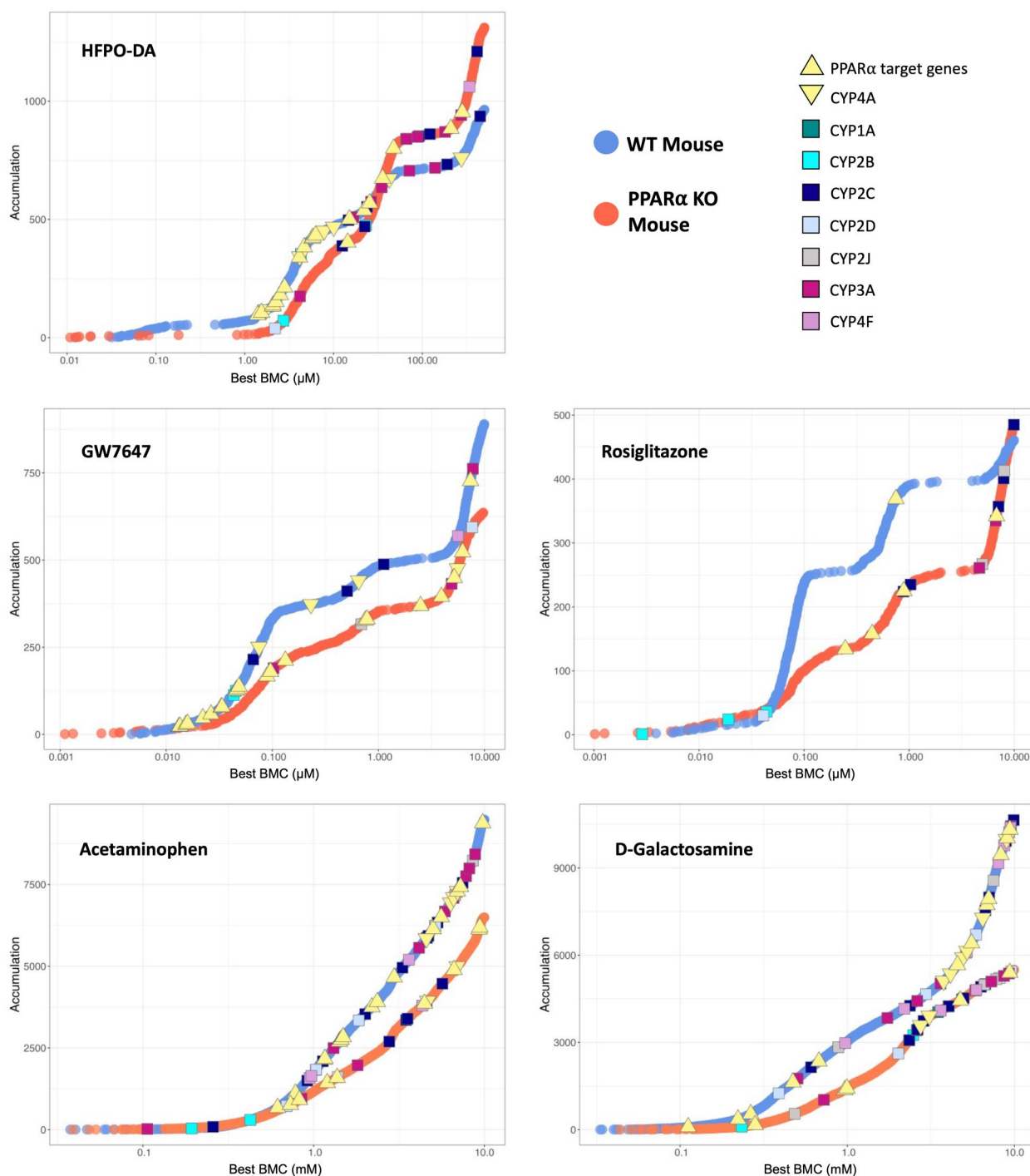


Figure 6. Accumulation plots of best BMCs among significant concentration-responsive probes (best fit p -value $\geq .1$) in WT and PPAR α KO mouse hepatocytes at 24 h. Concentration-responsive probes are indicated by blue and orange points for WT and PPAR α KO hepatocytes, respectively. Best BMCs of PPAR α target genes and lipid metabolizing cytochrome P450's (CYPs) are annotated by color-coded shapes. PPAR α target genes consist of 12 genes identified as HFPO-DA and/or GW7647-interacting genes highlighted in the ToxPi key in Figure 3. CYP4A is set apart from the other lipid metabolizing CYPs (denoted by a yellow downward-facing triangle shape) because it is the target CYP for PPAR α .

in a hepatic model with increased lipids (eg, high-fat diet rodent model), CAR, and to a lesser extent PXR, can be activated to increase fatty acid metabolism (Finn et al., 2009; Hernandez et al., 2009). Similar to observations in high-fat diet rodent models, hepatic lipid accumulation also occurred in PPAR α KO mice treated with PPAR α agonists, WY-14,643, or clofibrate (Lee et al., 1995). In the current study, lipid metabolizing CYPs, including those regulated by CAR or PXR, were activated at similar or

slightly lower concentrations than PPAR α target genes in PPAR α KO hepatocytes treated with HFPO-DA or GW7647, providing some support for the induction of compensatory homeostatic mechanisms. However, it is unknown whether this induction was via direct (despite low affinity) and/or indirect (eg, crosstalk) receptor activation.

In contrast to the PPAR α -activating compounds (HFPO-DA and GW7647), the PPAR γ agonist rosiglitazone increased enrichment

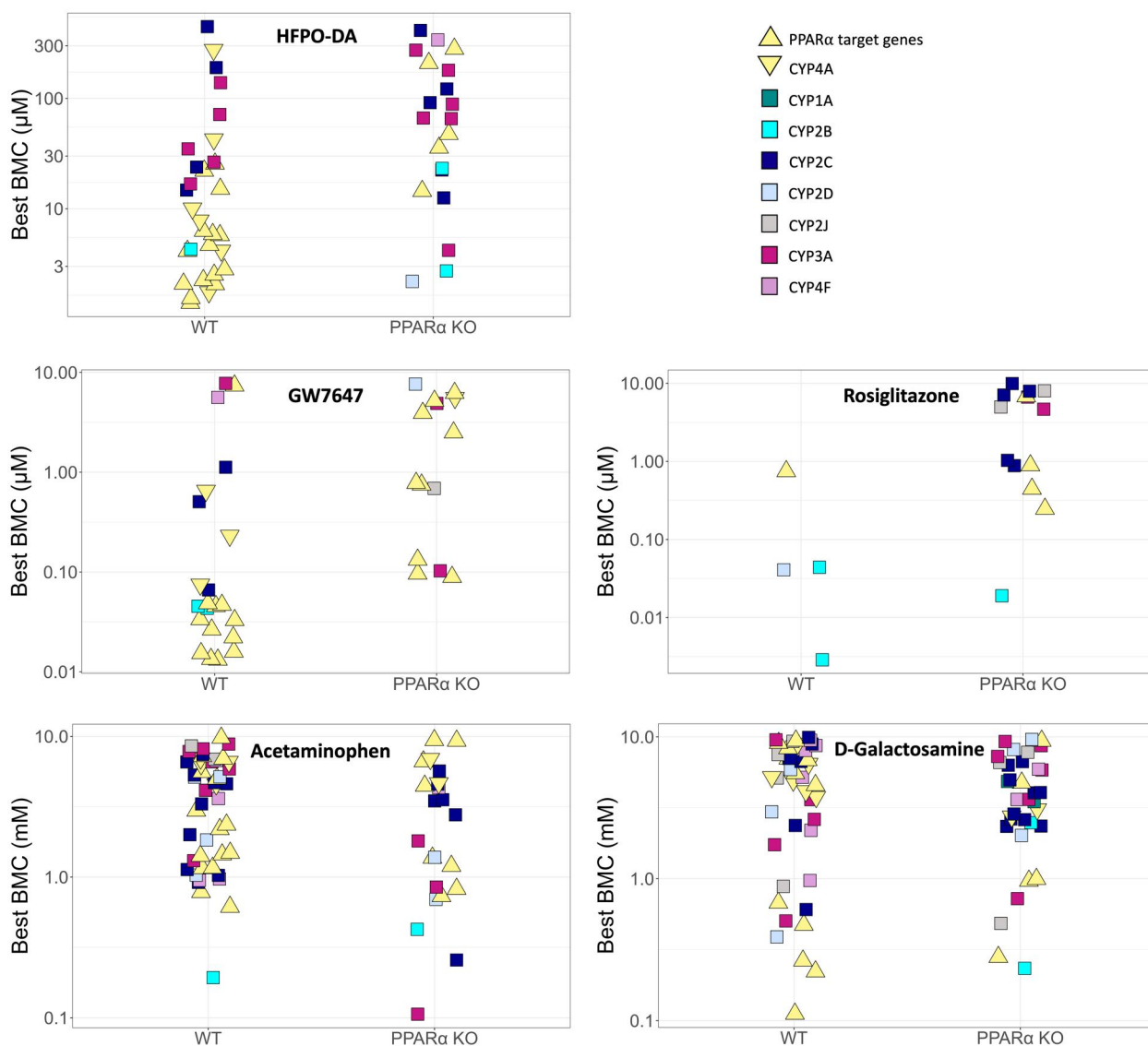


Figure 7. Best BMCs (best fit p -value $\geq .1$) for PPAR α target genes and lipid metabolizing CYPs in WT and PPAR α KO mouse hepatocytes at 24 h. Best BMCs are annotated by color-coded shapes. PPAR α target genes consist of 12 genes identified as HFPO-DA and/or GW7647-interacting genes highlighted in the ToxPi key in Figure 3. CYP4A is set apart from the other lipid metabolizing CYPs (denoted by a yellow downward-facing triangle shape) because it is the target CYP for PPAR α .

of fatty acid metabolism-related pathways at 12 h in PPAR α KO hepatocytes but not in WT hepatocytes. Although PPAR γ is expressed at low levels in the liver, hepatic activation of PPAR γ promotes energy storage through increased lipogenesis, whereas PPAR α activation promotes the release of energy via fatty acid oxidation and thermogenesis (Wang et al., 2020). Given these competing roles of energy homeostasis in the liver, it is conceivable that in the absence of PPAR α , rosiglitazone is more active in PPAR α KO hepatocytes and induces a greater transcriptomic response than in WT hepatocytes. Moreover, unlike WT hepatocytes, where pathway-level responses for HFPO-DA, GW7647, and rosiglitazone-treated hepatocytes were similar between HFPO-DA and GW7647-treated hepatocytes but different from rosiglitazone-treated hepatocytes, greater similarity was observed across pathway-level responses in rosiglitazone, HFPO-DA and GW7647-treated PPAR α KO hepatocytes, especially at higher concentrations and later timepoints. Despite being potent activators of human, rat, and mouse PPAR α (Behr et al.,

2020; Nielsen et al., 2022), HFPO-DA and GW7647 can also activate PPAR γ in transactivation assays, albeit with an approximately 100-fold (or more) lower potency compared with PPAR α (Behr et al., 2020; Brown et al., 2001; Evans et al., 2022). Thus, in the absence of PPAR α , at high concentrations and longer exposure durations, PPAR γ might be activated by HFPO-DA and GW7647. However, as described below, due to toxicokinetic differences between *in vitro* and *in vivo* experimental systems, compensatory responses observed in PPAR α KO hepatocytes treated with HFPO-DA or GW7647 are not anticipated *in vivo*. In contrast to results for rosiglitazone, no overlap in pathway enrichment was observed between HFPO-DA-treated hepatocytes and hepatocytes treated with cytotoxic agents, regardless of hepatocyte genotype, providing further support that HFPO-DA does not act through a cytotoxic MOA (Heintz et al., 2023).

In PPAR α KO hepatocytes, both GW7647 and HFPO-DA exhibited transient low-dose effects at 12 and 24 h, respectively. HFPO-DA appeared to induce changes related to protein degradation,

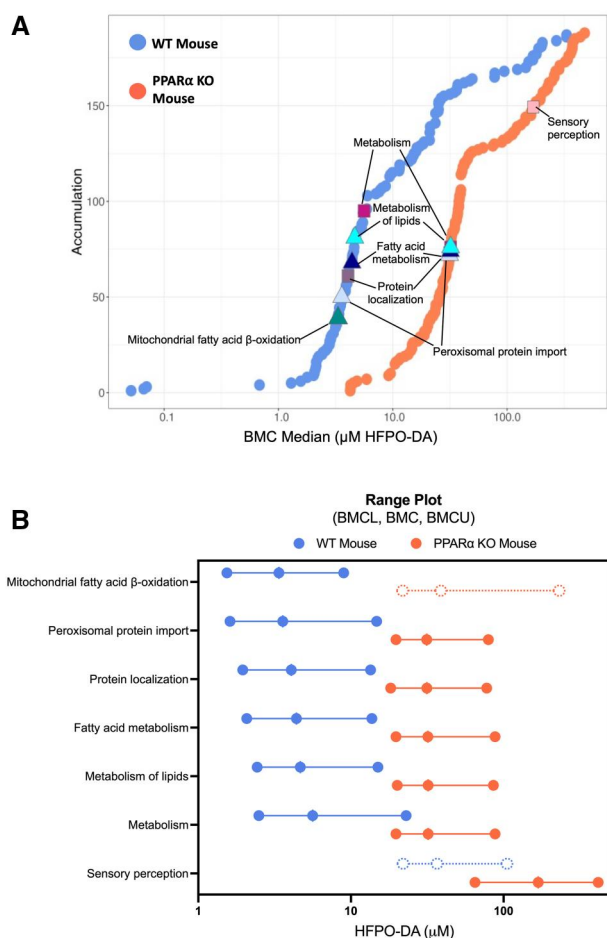


Figure 8. Pathway enrichment of significant concentration-responsive genes in HFPO-DA-treated WT (blue points) and PPAR α KO (orange points) mouse hepatocytes at 24 h. (A) Accumulation plots of median BMCs for significantly enriched pathways (Fisher's exact 2-tail <0.1). The top 6 most significantly enriched signaling pathways among concentration-responsive probes for HFPO-DA are annotated by color-coded shapes. (B) Range plots (median BMCL, median BMC, median BMCU) for the top 6 most significantly enriched signaling pathways (solid lines and circles) in WT and/or PPAR α KO hepatocytes treated with HFPO-DA at 24 h. Mitochondrial fatty acid β -oxidation and sensory perception signaling pathways were also significantly enriched in PPAR α KO and WT hepatocytes, respectively (indicated by dashed lines and circles), but were not among the top 6 most significant.

whereas GW7647 appeared to affect mitochondrial fatty acid β -oxidation. Whether these low-dose changes are the result of experimental factors (eg, handling issues), transcriptomic “noise,” or true biological responses is unclear. Interestingly, PPARs and other nuclear receptors are intricately controlled by the ubiquitin proteasome system (UPS), and each has unique responses to ligands—including stabilization of function, targeting for degradation, or, in the case of PPAR α , transient stabilization and subsequent degradation (Genini et al., 2008). In mice, exposure to clofibrate for 2 weeks has been shown to decrease expression of murine double minute 2 (*Mdm2*), an E3 ubiquitin ligase that binds to and regulates PPAR α , in WT mice but not PPAR α KO mice indicating a potential negative feedback loop to control PPAR α activation in the presence of a ligand (Gopinathan et al., 2009). These complex interactions between ligands, receptors, and coactivators/regulators (eg, *Mdm2*) might partially explain the apparent nonmonotonic (and different)

transcriptomic changes observed at low and high doses, which might be more apparent in the absence of PPAR α .

Interestingly, available *in vivo* studies in PPAR α KO mice have virtually no transcriptomic response (eg, few to no significant DEGs and no pathway-level response) following subacute or chronic exposures to established PPAR α agonists including WY-14,643 or GW7647 (Foreman et al., 2021; Rakhshandehroo et al., 2007). In addition, transcriptomic responses for HFPO-DA have also been examined in PPAR α KO mice administered a high-fat diet in combination with a low dose (0.3 mg/kg-bw/day) of HFPO-DA for 20 weeks. Although there was no negative control for the high-fat diet in this study, the authors determined that effects of HFPO-DA exposure on hepatic gene expression were dependent on PPAR α , due to “no significant gene regulation” by HFPO-DA in PPAR α KO mice (Attema et al., 2022). These results suggest that the delayed transcriptomic response observed *in vitro* for HFPO-DA and GW7647-treated PPAR α KO hepatocytes may be a consequence of the experimental system used. *In vivo*, chemical toxicokinetics can greatly affect the amount and duration of exposure in a specific tissue or cell type; whereas *in vitro*, the exposure is typically more controlled and constant, and when under stable conditions (eg, no chemical precipitation or volatilization) generally only differs if the test chemical is metabolized. For example, HFPO-DA is absorbed and rapidly eliminated in the urine of rats, mice, and monkeys, with an elimination half-life on the order of hours. In addition, HFPO-DA is not metabolized by rodent liver *in vitro* or *in vivo* (Gannon et al., 2016). To our knowledge, the toxicokinetics of GW7647 have not been investigated, however, the elimination half-life of GW7647 is also expected to be on the order of hours, similar to PPAR α agonist drugs (eg, fenofibrate; Chapman, 1987). Thus, the delayed compensatory responses observed *in vitro* for HFPO-DA and GW7647 in PPAR α KO hepatocytes are not anticipated *in vivo* in PPAR α KO mice due to the rapid elimination of these chemicals.

The *in vitro* system used in this study is best suited for examining early key events or molecular initiating events in the HFPO-DA MOA. The lack of concordance between HFPO-DA and cytotoxic agents in both WT and PPAR α KO hepatocytes indicates that liver effects observed in mice following HFPO-DA exposure are not the result of a cytotoxic MOA. With regard to support for a PPAR α MOA, the *in vitro* system herein is primarily capable of addressing Key Event 1 (PPAR α activation). An assessment of downstream key events (ie, alteration of cell growth pathways, perturbation of cell growth and survival, and selective clonal expansion of preneoplastic foci cells) is not feasible in cultured hepatocytes lacking nonparenchymal cells (eg, Kupffer cells) that facilitate cell proliferation (McMullen et al., 2020; Szalowska et al., 2014). Because the influence of PPAR α genotype on alteration of cell growth and survival cannot be readily assessed *in vitro*, *in vivo* studies are currently underway to further address Key Event 1 and subsequent key events in WT and PPAR α KO mice. In addition to transcriptomic analyses, these *in vivo* studies will include examination of phenotypic responses (eg, histopathological changes, serum liver enzymes) to further inform MOA.

In summary, the study design herein allows for the investigation of PPAR α -dependent and independent mechanisms across several chemicals, concentrations, and timepoints. The similar transcriptomic signaling patterns between HFPO-DA and an established PPAR α agonist (GW7647) in both WT and PPAR α KO hepatocytes support a shared MOA for both chemicals *in vitro* and presumably *in vivo*. These findings also provide mechanistic insight as to what happens in PPAR α KO mouse hepatocytes when treated with PPAR α and PPAR γ activators. PPAR signaling

and fatty acid metabolism-related pathways are mediated more efficiently in WT hepatocytes treated with HFPO-DA and GW7647, however, similar transcriptomic signaling potentially mediated by compensatory responses was also observed in the absence of PPAR α , albeit weaker and delayed. In contrast, rosiglitazone, appears more active in the absence of the PPAR α , likely due to the competing roles between PPAR α and PPAR γ in the liver for energy homeostasis.

Supplementary data

Supplementary data are available at *Toxicological Sciences* online.

Acknowledgments

The authors thank Dr James E. Klaunig for his support during early discussions in the design of this study.

Funding

The Chemours Company FC, LLC. Chemours was given the opportunity to review the draft manuscript. The purpose of this review by the funder was for the authors to receive input on the clarity of the science presented but not on the interpretation of research results. The authors' scientific conclusions and professional judgments were not subject to the funder's control; the contents of this manuscript solely reflect the view of the authors.

Declaration of conflicting interests

The authors declared the following potential perceived conflicts of interest with respect to the research, authorship, and/or publication of this article: The authors include employees of ToxStrategies LLC, a private consulting firm that provides services to private and public organizations for toxicology, epidemiology, and risk assessment issues. The research reported in this article was conducted during the normal course of employment.

Data availability

RNA sequencing data are publicly available at NCBI's Gene Expression Omnibus (<https://www.ncbi.nlm.nih.gov/geo/>) (GEO series accession number GSE248251). All Supplementary Files 1–6 are available at DOI: 10.5061/dryad.pc866t1wp.

References

- Attema, B., Janssen, A. W. F., Rijkers, D., van Schothorst, E. M., Hooiveld, G., and Kersten, S. (2022). Exposure to low-dose perfluorooctanoic acid promotes hepatic steatosis and disrupts the hepatic transcriptome in mice. *Mol. Metab.* **66**, 101602.
- Behr, A. C., Plinsch, C., Braeuning, A., and Buhrke, T. (2020). Activation of human nuclear receptors by perfluoroalkylated substances (PFAS). *Toxicol. In Vitro* **62**, 104700.
- Brown, P. J., Stuart, L. W., Hurley, K. P., Lewis, M. C., Winegar, D. A., Wilson, J. G., Wilkison, W. O., Ittoop, O. R., and Willson, T. M. (2001). Identification of a subtype selective human PPAR α agonist through parallel-array synthesis. *Bioorg. Med. Chem. Lett.* **11**, 1225–1227.
- Chapman, M. J. (1987). Pharmacology of fenofibrate. *Am. J. Med.* **83**, 21–25.
- Chappell, G. A., Thompson, C. M., Wolf, J. C., Cullen, J. M., Klaunig, J. E., and Haws, L. C. (2020). Assessment of the mode of action underlying the effects of GenX in mouse liver and implications for assessing human health risks. *Toxicol. Pathol.* **48**, 494–508.
- Corton, J. C., Cunningham, M. L., Hummer, B. T., Lau, C., Meek, B., Peters, J. M., Popp, J. A., Rhomberg, L., Seed, J., and Klaunig, J. E. (2014). Mode of action framework analysis for receptor-mediated toxicity: The peroxisome proliferator-activated receptor alpha (PPAR α) as a case study. *Crit. Rev. Toxicol.* **44**, 1–49.
- Corton, J. C., Peters, J. M., and Klaunig, J. E. (2018). The PPAR α -dependent rodent liver tumor response is not relevant to humans: Addressing misconceptions. *Arch. Toxicol.* **92**, 83–119.
- Costello, E., Rock, S., Stratakis, N., Eckel, S. P., Walker, D. I., Valvi, D., Cserbik, D., Jenkins, T., Xanthakos, S. A., Kohli, R., et al. (2022). Exposure to per- and polyfluoroalkyl substances and markers of liver injury: A systematic review and meta-analysis. *Environ. Health Perspect.* **130**, 46001.
- Cox, C. S., McKay, S. E., Holmbeck, M. A., Christian, B. E., Scortea, A. C., Tsay, A. J., Newman, L. E., and Shadel, G. S. (2018). Mitohormesis in mice via sustained basal activation of mitochondrial and antioxidant signaling. *Cell Metab.* **28**, 776–786.e775.
- Evans, N., Conley, J. M., Cardon, M., Hartig, P., Medlock-Kakaley, E., and Gray, L. E. Jr. (2022). In vitro activity of a panel of per- and polyfluoroalkyl substances (PFAS), fatty acids, and pharmaceuticals in peroxisome proliferator-activated receptor (PPAR) alpha, PPAR gamma, and estrogen receptor assays. *Toxicol. Appl. Pharmacol.* **449**, 116136.
- Finn, R. D., Henderson, C. J., Scott, C. L., and Wolf, C. R. (2009). Unsaturated fatty acid regulation of cytochrome p450 expression via a car-dependent pathway. *Biochem. J.* **417**, 43–54.
- Foreman, J. E., Chang, S. C., Ehresman, D. J., Butenhoff, J. L., Anderson, C. R., Palkar, P. S., Kang, B. H., Gonzalez, F. J., and Peters, J. M. (2009). Differential hepatic effects of perfluorobutyrate mediated by mouse and human PPAR-alpha. *Toxicol. Sci.* **110**, 204–211.
- Foreman, J. E., Koga, T., Kosyk, O., Kang, B. H., Zhu, X., Cohen, S. M., Billy, L. J., Sharma, A. K., Amin, S., Gonzalez, F. J., et al. (2021). Diminished hepatocarcinogenesis by a potent, high-affinity human PPAR α agonist in PPAR α -humanized mice. *Toxicol. Sci.* **183**, 70–80.
- Gannon, S. A., Fasano, W. J., Mawn, M. P., Nabb, D. L., Buck, R. C., Buxton, L. W., Jepson, G. W., and Frame, S. R. (2016). Absorption, distribution, metabolism, excretion, and kinetics of 2,3,3,3-tetrafluoro-2-(heptafluoropropoxy)propanoic acid ammonium salt following a single dose in rat, mouse, and cynomolgus monkey. *Toxicology* **340**, 1–9.
- Genini, D., Carbone, G. M., and Catapano, C. V. (2008). Multiple interactions between peroxisome proliferator-activated receptors and the ubiquitin-proteasome system and implications for cancer pathogenesis. *PPAR Res.* **2008**, 195065.
- Gopinathan, L., Hannon, D. B., Peters, J. M., and Vanden Heuvel, J. P. (2009). Regulation of peroxisome proliferator-activated receptor-alpha by MDM2. *Toxicol. Sci.* **108**, 48–58.
- Heintz, M. M., Chappell, G. A., Thompson, C. M., and Haws, L. C. (2022). Evaluation of transcriptomic responses in livers of mice exposed to the short-chain pfas compound HFPO-DA. *Front. Toxicol.* **4**, 937168.
- Heintz, M. M., Haws, L. C., Klaunig, J. E., Cullen, J. M., and Thompson, C. M. (2023). Assessment of the mode of action underlying development of liver lesions in mice following oral exposure to HFPO-DA and relevance to humans. *Toxicol. Sci.* **192**, 15–29.
- Heintz, M. M., Klaren, W. D., East, A. W., Haws, L. C., McGreal, S. R., Campbell, R. R., and Thompson, C. M. (2024). Comparison of transcriptomic profiles between HFPO-DA and prototypical PPAR α , PPAR γ , and cytotoxic agents in mouse, rat, and pooled human hepatocytes. *Toxicol. Sci.* **200**, 165–182.

- Hernandez, J. P., Mota, L. C., and Baldwin, W. S. (2009). Activation of car and PXR by dietary, environmental and occupational chemicals alters drug metabolism, intermediary metabolism, and cell proliferation. *Curr. Pharmacogenomics Person. Med.* **7**, 81–105.
- Kasano-Camones, C. I., Takizawa, M., Ohshima, N., Saito, C., Iwasaki, W., Nakagawa, Y., Fujitani, Y., Yoshida, R., Saito, Y., Izumi, T., et al. (2023). PPAR α activation partially drives NAFLD development in liver-specific Hnf4a-null mice. *J. Biochem.* **173**, 393–411.
- Lee, S. S., Pineau, T., Drago, J., Lee, E. J., Owens, J. W., Kroetz, D. L., Fernandez-Salguero, P. M., Westphal, H., and Gonzalez, F. J. (1995). Targeted disruption of the alpha isoform of the peroxisome proliferator-activated receptor gene in mice results in abolishment of the pleiotropic effects of peroxisome proliferators. *Mol. Cell. Biol.* **15**, 3012–3022.
- Love, M. I., Huber, W., and Anders, S. (2014). Moderated estimation of fold change and dispersion for RNA-seq data with DESeq2. *Genome Biol.* **15**, 550.
- McMullen, P. D., Bhattacharya, S., Woods, C. G., Pendse, S. N., McBride, M. T., Soldatow, V. Y., Deisenroth, C., LeCluyse, E. L., Clewell, R. A., and Andersen, M. E. (2020). Identifying qualitative differences in PPAR α signaling networks in human and rat hepatocytes and their significance for next generation chemical risk assessment methods. *Toxicol. In Vitro* **64**, 104463.
- Mudra, D. R., and Parkinson, A. (2001). Preparation of hepatocytes. *Curr. Protoc. Toxicol. Chapter* **14**, Unit 14.2.
- Nakagawa, T., Ramdhan, D. H., Tanaka, N., Naito, H., Tamada, H., Ito, Y., Li, Y., Hayashi, Y., Yamagishi, N., Yanagiba, Y., et al. (2012). Modulation of ammonium perfluorooctanoate-induced hepatic damage by genetically different PPAR α in mice. *Arch. Toxicol.* **86**, 63–74.
- Nielsen, G., Heiger-Bernays, W. J., Schlezinger, J. J., and Webster, T. F. (2022). Predicting the effects of per- and polyfluoroalkyl substance mixtures on peroxisome proliferator-activated receptor alpha activity in vitro. *Toxicology* **465**, 153024.
- NTP. (2018). *NTP Research Report on National Toxicology Program Approach to Genomic Dose-Response Modeling. Research Report 5*. U.S. Department of Health and Human Services, Research Triangle Park, NC.
- Phillips, J. R., Svoboda, D. L., Tandon, A., Patel, S., Sedykh, A., Mav, D., Kuo, B., Yauk, C. L., Yang, L., Thomas, R. S., et al. (2019). BMDEExpress 2: Enhanced transcriptomic dose-response analysis workflow. *Bioinformatics* **35**, 1780–1782.
- Rakhshandehroo, M., Sanderson, L. M., Matilainen, M., Stienstra, R., Carlberg, C., de Groot, P. J., Müller, M., and Kersten, S. (2007). Comprehensive analysis of PPARalpha-dependent regulation of hepatic lipid metabolism by expression profiling. *PPAR Res.* **2007**, 26839.
- Rosen, M. B., Lee, J. S., Ren, H., Vallanat, B., Liu, J., Waalkes, M. P., Abbott, B. D., Lau, C., and Corton, J. C. (2008). Toxicogenomic dissection of the perfluorooctanoic acid transcript profile in mouse liver: Evidence for the involvement of nuclear receptors PPAR alpha and car. *Toxicol. Sci.* **103**, 46–56.
- Szalowska, E., van der Burg, B., Man, H. Y., Hendriksen, P. J., and Peijnenburg, A. A. (2014). Model steatogenic compounds (amiodarone, valproic acid, and tetracycline) alter lipid metabolism by different mechanisms in mouse liver slices. *PLoS One* **9**, e86795.
- Thompson, C. M., Fitch, S. E., Ring, C., Rish, W., Cullen, J. M., and Haws, L. C. (2019). Development of an oral reference dose for the perfluorinated compound GenX. *J. Appl. Toxicol.* **39**, 1267–1282.
- USEPA. (2021). *Human Health Toxicity Values for Hexafluoropropylene Oxide (HFPO) Dimer Acid and Its Ammonium Salt (CASRN 13252-13-6 and CASRN 62037-80-3) Also Known As “GenX Chemicals”* EPA Document Number: 822r-21-010. Washington, DC: U.S. Environmental Protection Agency Office of Water (4304T) Health and Ecological Criteria Division.
- Varemo, L., Nielsen, J., and Nookaew, I. (2013). Enriching the gene set analysis of genome-wide data by incorporating directionality of gene expression and combining statistical hypotheses and methods. *Nucleic Acids Res.* **41**, 4378–4391.
- Wang, Y., Nakajima, T., Gonzalez, F. J., and Tanaka, N. (2020). PPARs as metabolic regulators in the liver: Lessons from liver-specific PPAR-null mice. *Int. J. Mol. Sci.* **21**, 2061.
- Wolf, D. C., Moore, T., Abbott, B. D., Rosen, M. B., Das, K. P., Zehr, R. D., Lindstrom, A. B., Strynar, M. J., and Lau, C. (2008). Comparative hepatic effects of perfluorooctanoic acid and WY 14,643 in PPAR-alpha knockout and wild-type mice. *Toxicol. Pathol.* **36**, 632–639.
- Yeakley, J. M., Shepard, P. J., Goyena, D. E., VanSteenhouse, H. C., McComb, J. D., and Seligmann, B. E. (2017). A trichostatin A expression signature identified by TempO-Seq targeted whole transcriptome profiling. *PLoS One* **12**, e0178302.